Wave-Field Shaping in Cavities: Waves Trapped in a Box with Controllable Boundaries

Matthieu Dupré, Philipp del Hougne, Mathias Fink, Fabrice Lemoult, and Geoffroy Lerosey*
Institut Langevin, ESPCI ParisTech and CNRS UMR 7587, 1 rue Jussieu, 75005 Paris, France
(Received 26 March 2015; published 2 July 2015)

Electromagnetic cavities are used in numerous domains of applied and fundamental physics, from microwave ovens and electromagnetic compatibility to masers, quantum electrodynamics (QED), and quantum chaos. The wave fields established in cavities are statically fixed by their geometry, which are usually modified by using mechanical parts like mode stirrers in reverberation chambers or screws in masers and QED. Nevertheless, thanks to integral theorems, tailoring the cavity boundaries theoretically permits us to design at will the wave fields they support. Here, we show in the microwave domain that it is achievable dynamically simply by using electronically tunable metasurfaces that locally modify the boundaries, switching them in real time from Dirichlet to Neumann conditions. We prove that at a high modal density, counterintuitively, it permits us to create wave patterns presenting hot spots of intense energy. We explain and model the physical mechanism underlying the concept, which allows us to find a criterion ensuring that modifying parts of a cavity's boundaries turn it into a completely different one. We finally prove that this approach even permits us, in the limiting case where the cavity supports only well-separated resonances, to choose the frequencies at which the latter occur.

DOI: 10.1103/PhysRevLett.115.017701 PACS numbers: 84.40.-x, 41.20.Jb, 42.25.Dd

Cavities, because they trap waves for long times due to their reflecting walls, are used in a vast number of scientific domains [1–10]. Indeed, in these closed media and due to interferences, the free space continuum of solutions becomes a discrete set of stationary eigenmodes ψ_n of eigenfrequencies ω_n. These enhanced stationary fields are commonly used in fundamental physics to increase wave-matter interactions [3] or in electromagnetic compatibility to test electronic devices [1]. Yet the eigenmodes and associated eigenfrequencies of a cavity are imposed and hence statically fixed by its geometrical properties through the boundary conditions [11]. This explains why mechanical parts are ordinarily used to physically modify the properties of reverberant media: rotating trays in microwave ovens, mode stirrers in reverberation chambers, or even screws in masers and QED electromagnetic cavities. In this work, we break these paradigms by showing that one can control at will and in real time the wave fields created by antennas in cavities by tailoring only their boundaries without any mechanical component. This is achieved through the use of a binary tunable reflecting metasurface [12,13] [denoted the spatial microwave modulator (SMM)], which is part of the frontiers of the cavity, and can switch dynamically its boundary conditions from Dirichlet to Neumann.

We perform our demonstrations in the microwave domain, using antennas placed inside reverberant metallic cavities. For the sake of completeness, we demonstrate our findings with a disordered cavity [Fig. 1(a)] that allows achieving statistical averaging. For large enough cavities and at the angular frequency ω, the spectral density of modes $\rho(\omega)$, which defines the average frequency spacing between eigenmodes, is asymptotically equal to the Weyl law [5,15–18] for a three-dimensional and polarized electromagnetic field:

$$\rho(\omega) = \frac{1}{\pi^2} V \frac{\omega^2}{c_0^3}, \tag{1}$$

where V is the volume of the cavity and c_0 the speed of light in vacuum.

Real cavities always include some dissipation, due to Ohmic losses or leakage for partially radiative cavities, and hence the eigenmodes become resonances with linewidths Γ_n or, equivalently, quality factors $Q_n = 2\omega_n/\Gamma_n$. When one considers a given frequency, there may be several modes overlapping due to the widening of each Lorentzian. This number of modes $N(\omega)$ strongly depends on the cavity quality factor, which is statistically the average over the Q_n, and on the mode density $\rho(\omega)$. It may vary from much larger than unity to smaller than unity (meaning well-separated resonances) as schemed in Figs. 1(b)–1(d). On average, it is estimated by

$$N(\omega) = \rho(\omega)\langle\Gamma_n\rangle = \frac{2}{\pi^2}\frac{V}{Q}\left(\frac{\omega}{c_0}\right)^3. \tag{2}$$

The simplest way to probe the wave fields established inside cavities consists in measuring the transmission between a source antenna S and a receiver one R, both placed inside it, as depicted in Fig. 1(a). The transmission $t(\omega)$ is the Green function between those two points, which is the sum of the $N(\omega)$ contributing modes [19–21]:

$$t(\omega) = \sum_{n=1}^{N(\omega)} \frac{\psi_n(\mathbf{r}_S)\psi_n^*(\mathbf{r}_R)}{\omega^2 - \omega_n^2 + i\omega\Gamma_n}. \tag{3}$$

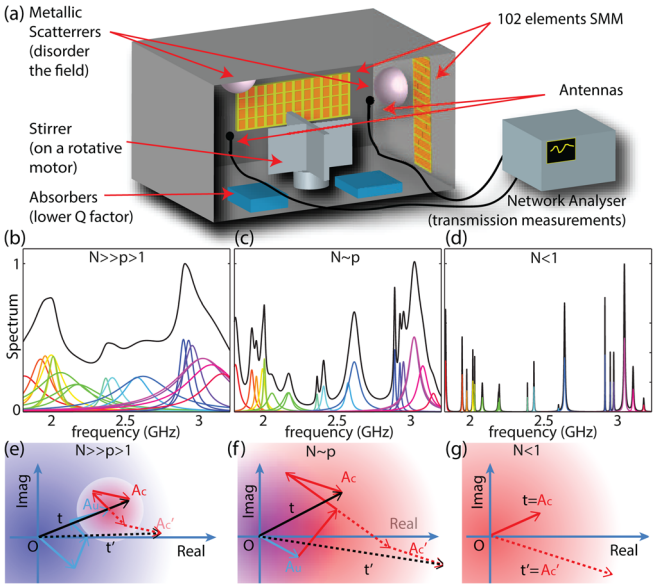

FIG. 1 (color online). Concept. (a) Experimental setup [14]: cavity dimensions $1.45 \times 1 \times 0.75$ m^3. (b)–(d) Schematic contribution of the resonances (color lines) to the total transmission (black line) for (b) a large number of modes, (c) the limit of our model, and (d) with N lower than 1. (e)–(g) Schematic view of the random walks of the N contributing modes corresponding to (b)–(d) when the sign of p modes out of N can be controlled. A_c is the sum of the p controlled modes, while A_u is the sum of $N-p$ uncontrolled modes. The total transmission t (in black) corresponds to the sum of A_c with A_u. Plain (dashed) arrows: before (after) optimization.

Since our experiments take place in a disordered cavity, the eigenmodes and hence any linear combination of them are also disordered; namely, their spatial profile looks like an optical speckle. The transmission is thus the summation of $N(\omega)$ statistically independent spatial wave patterns, that we call spatial degrees of freedom. By dropping the frequency dependence, this transmission coefficient can be written as a sum of N complex numbers with random amplitudes and phases, namely, phasors:

$$t = \sum_{k=1}^{N} t_k e^{i\theta_k}. \tag{4}$$

We will now show that we can actually control these spatial degrees of freedom in order to tune the transmission between antennas or, in other words, to shape the wave fields inside the cavity, just by modifying the boundaries of the cavity. We place the SMM on part of the cavity boundaries [Fig. 1(a)]. It is composed of 102 half-wavelength-square areas that are patch resonators [12], which can be turned on and off resonance by using diodes. An electronic board can therefore switch them from almost perfect electric conductors to magnetic conductors, corresponding, respectively, to Dirichlet and Neumann boundary conditions for the electric field [14]. Using the SMM, we can hence control p spatial degrees of freedom of the wave field, with p ranging from 0 to 102 at the operating frequency of 2.47 GHz, if we assume the boundary elements statistically independent. This hypothesis should be valid, since all elements are separated by the coherence length of the field inside the disordered cavity, i.e., half a wavelength [14]. We will use this SMM alongside an algorithm developed in the optical domain to focus light through multiple scattering media using spatial light modulators, a technique known as wavefront shaping [13,22–25]. Similarly, in our wave-field shaping experiments, we iteratively test every element of the SMM to obtain the best transmission between S and R [14]. Performing this optimization is actually a very convenient way to investigate the physics of waves trapped in these cavities: We test several hundreds of distinct cavities in real time thanks to the SMM, which allows us to link the results to the statistical parameters describing disordered cavities.

From a mathematical point of view, changing the boundary conditions of p elements of the SMM amounts to controlling the sign of p modes out of N, hence leaving $(N-p)$ uncontrolled ones [14]. Such a sum of random phasors [26] can be represented in the complex space as a sum of vectors of random amplitude t_k and phase θ_k, similarly to a 2D random walk [Figs. 1(e) and 1(f)]. The transmission is then the sum of two independent phasors, an uncontrolled one A_u, which is constant for a given cavity, and a phase-controlled one A_c:

$$t = A_u + A_c = \sum_{k=1}^{N-p} t_k e^{i\theta_k} + \sum_{k=1}^{p} t_k e^{i\theta_k}. \tag{5}$$

Comparing the root mean square values of A_u and A_c, one identifies three different regimes of control of the cavity. (i) The first one corresponds to $N \gg p$ [Fig. 1(b)] or, equivalently, to $A_u \gg A_c$ [Fig. 1(e)]. In this case, we will show that the transmission between the source and the receiver can be noticeably increased thanks to the SMM, hence resulting in focused wave fields. (ii) A transition occurs when A_c becomes comparable to A_u [Fig. 1(f)], that is, when the number of available spatial degrees of freedom equals that of the controlled ones, i.e., $N \approx p$ [Fig. 1(c)]. In this case, we completely control the cavity by modifying a few of its boundary conditions, and we can turn it into a statistically different one. (iii) When N is further decreased, we may have no mode around the working frequency and a very low transmission [Fig. 1(d)]. In this regime, we will show that optimizing the transmission between two antennas amounts to finding the best cavity out of the 2^p available ones to create an eigenmode which is maximal at both antenna positions, at the working frequency [Fig. 1(g)]. Interestingly, from the experimental point of view, we can access all of those cases simply by modifying the cavity quality factor or its volume.

We start by considering case (i) where $N \gg p$ and use the optimization algorithm [13,22,24,25] with the

SMM to enhance the transmission between S and R. Figures 2(a) and 2(b) show typical spectra and averaged spectra of the transmitted energy between these antennas, before and after the optimization, respectively. The transmission between two antennas is increased by a factor of 10 on average, while on two other receiving antennas it remains constant. This proves that the originally randomly distributed wave field is turned into a focused one. A random walk approach gives a simple picture of this phenomenon. Before optimization, the transmission is a sum of N random phasors, since both controlled and uncontrolled modes are randomly oriented in the complex plane, and its extension is on average proportional to $\sqrt{N}$ [26,27]. However, the optimization aligns the p vectors in a given direction, which means that A_c becomes proportional to p, while A_u remains a random sum of phasors that is proportional to $\sqrt{N-p}$ [Figs. 1(b) and 1(e)]. We therefore define the enhancement η as the ratio between the average transmitted energy before and after optimization:

$$\eta = \frac{\langle |t|^2 \rangle_f}{\langle |t|^2 \rangle_i} \approx \left(\frac{\sqrt{N-p} + p}{\sqrt{N}} \right)^2. \tag{6}$$

An exact calculation [14] that accounts for the fact that we control only the sign of the p elements leads to the enhancement:

$$\eta = 1 + \frac{1}{\pi}\frac{p(p-1)}{N} + \frac{2C(p)}{N}\sqrt{(N-p)p}\sqrt{1+\frac{1}{\pi}(p-1)}, \tag{7}$$

where $C(p)$ is a positive function quickly converging towards 1.

In order to verify our model, we conduct a statistical series of experiments while independently varying the number of controlled elements p and the Q factor, that is, the number of modes [14]. For each value of p or Q, we perform 270 statistically independent optimizations. The averages of these optimizations are presented in Figs. 2(c) and 2(d). The enhancement tends to initially evolve in a quadratic way with the number of iterations, as expected from our theoretical model. We also notice that, at high Q factors, the enhancement curves converge much slowly. We attribute this to correlations between the p elements due to reverberation, a topic that will be the scope of future work.

In Figs. 2(e) and 2(f), we plot the average final enhancements obtained versus the two variables p and Q. We furthermore fit the obtained results with our theoretical model [14]. Yet we introduce a parameter α which weights the number of controlled elements p. We find a fitting parameter $\alpha = 0.3$ [more exactly, 0.27 for Fig. 2(e) and 0.34 for Fig. 2(f)]. This value lower than unity accounts for three different facts: The elements of the SMM dissipate about 50% of the incoming energy [12], their efficiency at

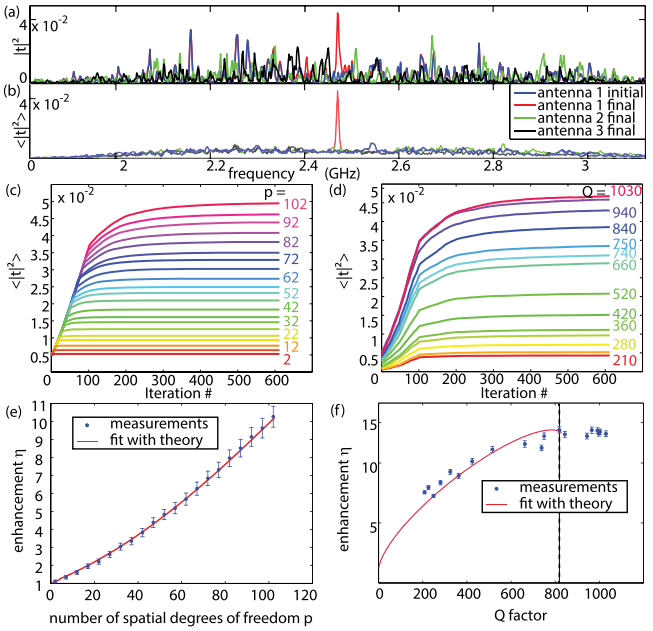

FIG. 2 (color online). Case (i), $N \gg p$. (a) Typical energy transmission between one emitter and three identical receivers (antennas 1–3), separated by more than a wavelength. Quality factor, $Q = 820$; number of SMM elements, $p = 102$. The blue (respectively, red) curve is the transmission before (respectively, after) optimization on receiver R (antenna 1). The black and green curves are the transmissions on antennas 2 and 3, respectively, after optimizing on the receiver R. (b) The same as (a), but averaged on the stirrer positions and on the initial state of the SMM. (c) Averaged transmission as a function of the iteration number of the algorithm for $Q = 820$ and varying p. (d) The same for varying Q and keeping $p = 102$. (e),(f) Final enhancement η versus p for $Q = 820$ and versus Q for $p = 102$. The theoretical fits correspond to Eq. (7) with p replaced by αp ($\alpha \approx 0.3$).

the operating frequency is not identical from element to element due to fabrication mismatches, and they act only on a single polarization of the electromagnetic field on the boundaries [14]. Yet the very good agreement between the experiments and Eq. (7) underlines the validity of the developed theoretical model.

We note that the fit of Fig. 2(f) stops at $Q > 850$ as it reaches the point $p = N$, which is the model limit, as we cannot control more degrees of freedom than are available in the experiment. In order to investigate deeper what happens near this model's edge, i.e., for case (ii) where $A_u \approx A_c$, we conduct a new series of experiments. This time, we do not use the mode stirrer, in order to keep the exact same cavity for all the experiments, but we change only its boundaries thanks to the SMM. Using 102 elements, we randomly pick 700 starting configurations of the SMM (out of the 2^{102} possible ones) and start the optimization process. We do so for different ratios of N/p [14], in order to investigate the role of the p controlled boundaries on the physics of the cavity. Figures 3(a)–3(c) show the measured initial and optimized transmissions in

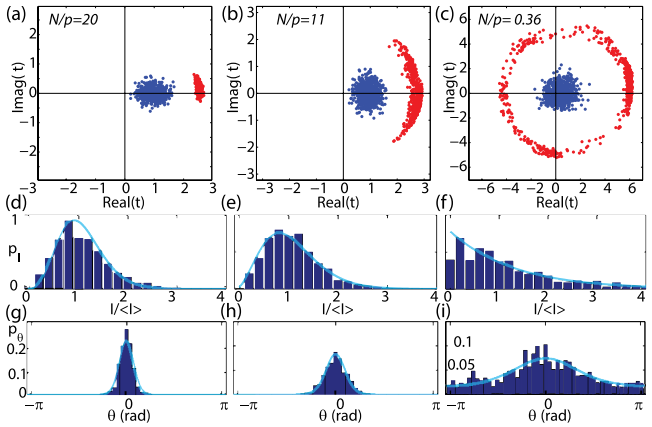

FIG. 3 (color online). From case (i) to (ii). (a)–(c) Initial (blue) and optimized (red) transmissions (normalized by the averaged initial transmission) for 700 initial configurations of the SMM for a single cavity, in the complex plane. From (a) to (c), we decrease N from large values ($A_u > A_c$) down to $N/p < 1$. (d)–(f) Initial intensity $|t^2|$ probability density function $p_I(I)$ for the three cases. (g)–(i) The same for the probability density function of the phase $p_\theta(\theta)$ [note the scale change in (i)].

the complex plane or so-called Fresnel representation. It is a direct picture of the random summation of the phasors we previously discussed, and the results show a markedly different behavior when N becomes lower than p. At this point, the amplitude of A_c becomes larger than A_u, which is fixed for a given cavity. Hence, the binary controlled sum of phasors becomes dominant and governs the cavity as schemed in Fig. 1(f). In this case, the initial (or final) phase of the transmission explores the entire complex circle: The SMM alone can arbitrarily govern the wave field. In other words, the cavity is turned into a completely different one just by changing part of its boundaries. This effect is even more visible from the optimized transmissions (red dots): The accessible angles clearly span a limited range at high N/p, while an entire circle is visited for the low ratio. We further realize a statistical study of the distribution of the intensity and phase of the measured transmissions before optimization. To do so, we first plot histograms of these distributions for the various cases. We notice that the histograms are rather different for the first two series of experiments than for the last one. Indeed, for $N/p \gg 1$, the intensity histograms show a maximum for a nonzero value, and the phase histograms are narrowly distributed around 0, while, for $N/p < 1$, the intensity probability peaks near the origin and the phase one is much flatter [Figs. 2(d)–2(i)]. These results are in very good agreement with the theory since, for $N/p \gg 1$, that is, for the very large sum of constant phasors with the small sum of random ones, the intensity probability density function is expected to be Rician modified and the phase one Gaussian [8,26]. On the contrary, if we sum only a random set of phasors, i.e., if the SMM controls the whole cavity, we anticipate an exponentially decreasing probability density function for the measured intensity and a constant one for the phase [8,26]. The theoretical curves calculated with N and p estimated from the measurements fit very well the histograms.

If N is further decreased such that the resonances become discrete, our previous model does not stand at all. In this limiting case (iii), there may be no resonance at the operating frequency [Fig. 1(d)]. However, we can still run optimizations of the transmission between two antennas. In order to perform these experiments, we have to drastically decrease N, which can be done only by reducing the modal density. Indeed, most of the dissipation in our experiments is due to the SMM, which limits the Q factor of the cavities (note nonetheless that almost lossless SMM are realizable). Therefore, we work with a small cavity and a miniature mode stirrer [Fig. 4(a)] and utilize the same setup as in Fig. 1(a) albeit with a smaller SMM consisting of eight elements. Figure 4(c) presents the transmission spectrum at intermediate steps of the optimization. We observe the creation of a resonance corresponding to an eigenmode around the working frequency. To verify the validity of our results, yet with a larger cavity, we finally perform finite element simulations using COMSOL MULTIPHYSICS. This allows us to reach the regime of low values of N, this time by using a very high Q factor and large ergodic cavity [28,29] [Fig. 4(b)]. The results of an optimized transmission [Fig. 4(d)] demonstrate that our approach still works in this case, as we have created a resonance at 2.47 GHz by optimizing the transmission between two points. These results assert that, at a low density of modes, we can finely tune the spectral properties of a cavity without any mechanical part. This approach, which paves the way to the design of real time electronically reconfigurable

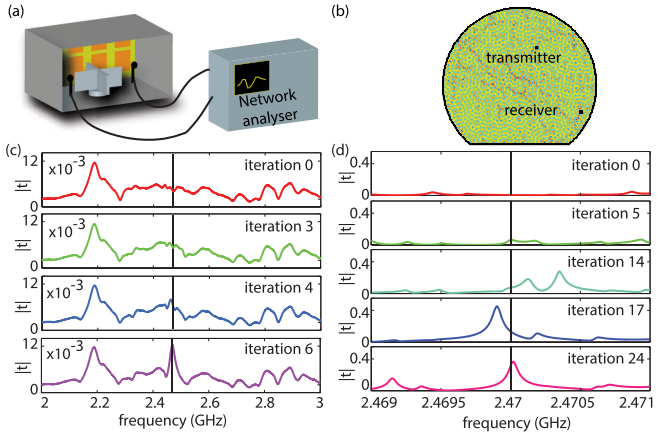

FIG. 4 (color online). Case (iii), $N < 1$. (a) Experimental setup. Cavity dimensions: 12 cm × 12 cm × 24 cm with an eight-element SMM. (b) The 2D simulated ergodic cavity of radius $20\lambda_0$. SMM of 20 elements. $Q = 10^5$. (c) Experimental transmission $|t|$ at low N for different optimization steps. (d) The same in simulations.

single mode cavities, will have many applications in fundamental physics [2–7].

In this Letter, we have studied and modeled the physics of waves trapped in reverberating cavities with dynamically controllable boundary conditions, by using a tunable metasurface as a spatial microwave modulator. Our results prove that, at high modal density, tailoring the boundaries of a cavity allows us to turn a randomly distributed wave field into a focused one, thus paving the way to real time and dynamical wave-field shaping in reverberating media [30,31], with potential applications in wireless communication [13] or electromagnetic compatibility. We have further shown that, when the number of modes is decreased, the cavity reaches a regime completely governed by the modulator where one can easily turn a given cavity into a different one. Finally, in a third regime where the resonances are clearly distinct, we have proven that we can create and finely tune the eigenmodes and eigenfrequencies of a cavity. Dynamically reconfigurable cavities will find many applications in applied and fundamental physics and shed light on very interesting mathematical problems.

M. D. acknowledges funding from French "Ministère de la Défense, Direction Générale de l'Armement." This work is supported by LABEX WIFI (Laboratory of Excellence within the French Program "Investments for the Future") under references ANR-10-LABX-24 and ANR-10-IDEX-0001-02 PSL$*$ and by Agence Nationale de la Recherche under reference ANR-13-JS09-0001-01.

*geoffroy.lerosey@espci.fr

[1] D. A. Hill, *Electromagnetic Fields in Cavities: Deterministic and Statistical Theories* (Wiley, New York, 2009).
[2] J.-B. Gros, O. Legrand, F. Mortessagne, E. Richalot, and K. Selemani, Wave Motion **51**, 664 (2014).
[3] D. E. McCumber, Phys. Rev. **130**, 675 (1963).
[4] H. Walther, B. T. H. Varcoe, B.-G. Englert, and T. Becker, Rep. Prog. Phys. **69**, 1325 (2006).
[5] M. C. Gutzwiller, J. Math. Phys. **12**, 343 (1971).
[6] H.-J. Stöckmann and J. Stein, Phys. Rev. Lett. **64**, 2215 (1990).
[7] H.-J. Stöckmann, *Quantum Chaos: An Introduction* (Cambridge University Press, Cambridge, 2007).
[8] S. Hemmady, X. Zheng, T. M. Antonsen, E. Ott, and S. M. Anlage, Phys. Rev. E **71**, 056215 (2005).
[9] P. So, S. M. Anlage, E. Ott, and R. N. Oerter, Phys. Rev. Lett. **74**, 2662 (1995).
[10] H. Cao and J. Wiersig, Rev. Mod. Phys. **87**, 61 (2015).
[11] M. E. Taylor, *Partial Differential Equations. II: Qualitative Studies of Linear Equations* (Springer, New York, 1996).
[12] N. Kaïna, M. Dupré, M. Fink, and G. Lerosey, Opt. Express **22**, 18881 (2014).
[13] N. Kaïna, M. Dupré, G. Lerosey, and M. Fink, Sci. Rep. **4**, 6693 (2014).
[14] See Supplemental Material at http://link.aps.org/supplemental/10.1103/PhysRevLett.115.017701 for the derivation of Eq. (7), the optimization algorithm, and experimental and numerical details.
[15] H. Weyl, *Nachrichten der Königlichen Gesellschaft der-Wissenschaften zu Göttingen* (Weidmannsche Buchhandlung, Berlin, 1911), pp. 110–117.
[16] W. Arendt, R. Nittka, W. Peter, and F. Steiner, *Weyl's Law: Spectral Properties of the Laplacian in Mathematics and Physics* (Wiley, Weinheim, 2009).
[17] R. Balian and B. Duplantier, Ann. Phys. (N.Y.) **104**, 300 (1977).
[18] S. Bittner, B. Dietz, R. Dubertrand, J. Isensee, M. Miski-Oglu, and A. Richter, Phys. Rev. E **85**, 056203 (2012).
[19] U. Kuhl, H.-J. Stöckmann, and R. Weaver, J. Phys. A **38**, 10433 (2005).
[20] J. Barthélemy, O. Legrand, and F. Mortessagne, Phys. Rev. E **71**, 016205 (2005).
[21] J. Barthélemy, O. Legrand, and F. Mortessagne, Europhys. Lett. **70**, 162 (2005).
[22] I. M. Vellekoop and A. P. Mosk, Opt. Lett. **32**, 2309 (2007).
[23] I. M. Vellekoop and A. P. Mosk, Opt. Commun. **281**, 3071 (2008).
[24] D. Akbulut, T. J. Huisman, E. G. van Putten, W. L. Vos, and A. P. Mosk, Opt. Express **19**, 4017 (2011).
[25] A. P. Mosk, A. Lagendijk, G. Lerosey, and M. Fink, Nat. Photonics **6**, 283 (2012).
[26] J. W. Goodman, *Speckle Phenomena in Optics* (Roberts, Englewood, 2010).
[27] J. W. Goodman, *Statistical Optics* (Wiley, New York, 2000).
[28] L. A. Bunimovich, Commun. Math. Phys. **65**, 295 (1979).
[29] S. Ree and L. E. Reichl, Phys. Rev. E **60**, 1607 (1999).
[30] F. Lemoult, G. Lerosey, J. de Rosny, and M. Fink, Phys. Rev. Lett. **103**, 173902 (2009).
[31] M. Dupré, M. Fink, and G. Lerosey, Phys. Rev. Lett. **112**, 043902 (2014).